Chapter 7

Microwave Absorption in Nanostructured Spinel Ferrites

Gabriela Vázquez-Victorio, Ulises Acevedo-Salas and Raúl Valenzuela

Additional information is available at the end of the chapter

http://dx.doi.org/10.5772/56058

1. Introduction

Magnetic Nanoparticles

Magnetic nanoparticles (MNPs) are playing a crucial role in an extensive number of potential applications and science fields. Nanotechnology industry is rapidly growing with the promise that it will lead to significant economic and scientific impacts on a wide range of areas, such as health care, nanoelectronics, environmental remediation. MNPs are mostly ferrites, i.e, transition metal oxides with ferric ions as main constituent. Although the magnetic properties of ferrites [1] are less intense than metal's, especially saturation magnetization, ferrites possess a large chemical stability (corrosion resistance), high electrical resistivity, and extended applicability at high magnetic field frequencies.

The use of MNPs for biological and clinical applications [2] is undoubtedly one of the most challenging research areas in the field of nanomaterials, involving the organized collaboration of research teams formed by physicists, chemists, biologists, physiciens. The advantages of MNPs are based on their nanoscale size, large surface area, tailoring of magnetic properties and negligible side effects in living tissues. These applications include drug delivery [3], magnetic hyperthermia [4], magnetic resonance imaging [5], biosensors [6]. A field related with microwave absorption is electromagnetic interference EMI [7], as the number of electromagnetic radiation sources has growth at an exponential rate. MNPs have found applications also in environmental fields, such as soil remediation [8] and heavy metal removal [9], as MNPs provide high surface area and specific affinity for heavy metal adsorption from aqueous systems.

The reduction in scale leads to strong changes in macroscopic properties. The main reason can be attributed to the enhanced importance of the surface atom fraction as compared with core atom fraction, as the material becomes a nanoparticle. A simple estimate reveals that

for a ~100 nm nanoparticle, surface atom fraction is about 6% of the total NP atoms, while for a ~5 nm NP this fraction can attain 78% [10]. Surface layer of materials exhibits different properties simply because these atoms have a very different structure than the core's. Surface atoms, for instance, have a reduced coordination number (unsatisfied bonding), crystal defects and modified crystal planes ("broken symmetry"). In the case of magnetically ordered materials (ferro, ferri, antiferromagnetic phases), additionally, several magnetic properties critically change at the nanometric scale. These properties are, for instance, the change from multidomain to single domain magnetic structure, domain wall thickness, the decrease in anisotropy energy giving rise to superparamagnetic phenomena. MNPs can thus exhibit many property changes with the reduction in size. Last (but no least), MNPs can show important macroscopic effects of interparticle magnetic interactions, which can involve additive forces (exchange), or attraction/repulsion (dipole).

Synthesis of MNPs

The most common method to synthesize MNPs are based on coprecipitation and microemulsion [11]. The coprecipitation method produces NPs by a pH change in a solution containing the desired metals in the form of nitrates or chlorides. Average size and size distribution, as well as shape depend on the pH and the ionic strength of the precipitating solution. In the microemulsion method, an aqueous metal solution phase is dispersed (entrapped) as microdroplets in a continuous oil phase within a micellar assembly of stabilizing surfactants. The advantage is that the microdroplets provide a confined space which limits the growth and agglomeration of NPs.

An emerging method for preparation of uniform NPs is the polyol technique, where metallic salts (acetates, oxalates), dissolved in an alcohol (such as diethylenglycol) are directly precipitated by high temperature decomposition [12]. This method can produce metals; by addition of a controlled amount of water, it can lead to oxide MNPs.

Spray and laser pyrolysis, with great commercial scale-up potential have been reported [13]. In spray pyrolysis, a solution of a ferric salt (and a reducing agent) is sprayed through a reactor to produce evaporation of the solvent within each droplet. In laser pyrolysis, the laser energy is used to heat a flowing mixture of gases leading to a chemical reaction. Under the appropriate conditions, homogeneous nucleation occurs and NPs are produced.

A different method utilizes high-energy ultrasound waves to create acoustic cavitations resulting in extremely hot spots. The sound waves produced by these cavities can lead to particle size reduction and hence the formation of NPs [14]. Other methods are based on electrochemical deposition of metal in a cathode [11], and also the use of magnetotactic bacteria [15].

Microwave absorption in MNPs

In this brief review, some of the recent developments in microwave absorption in MNPs. The response of ferromagnetic resonance (FMR) of MNPs (under different conditions) is first reviewed. FMR results on consolidated materials by spark plasma sintering (SPS) techniques are included, as this method allows the preparation of nanostructured ferrites (grains under

100 nm in size) with high densities. The behavior of electron paramagnetic resonance (EPR) of some relevant magnetically disordered MNPs systems is also presented. We devote a part of this review to the emerging low field microwave absorption technique (LFMA), which is a non-resonant method providing valuable information on magnetically-ordered materials. Results on MNPs in different aggregation states, as well as SPS-sintered materials are briefly reviewed.

As FMR [16] and EPR [17] techniques are well known, so no additional treatment of them is included here, except for some references.

2. Ferromagnetic resonance (FMR) in ferrite nanoparticles

Temperature and size dependences

One of the most studied phenomena on MNP's is the change of their FMR spectra as a function of temperature. The main parameters describing FMR signal are plotted versus temperature and eventually compared with the bulk counterpart, as an attempt to characterize the changes associated with the nanometric scale. Such parameters are generally peak-to-peak resonance linewidth, ΔH_{pp}, resonance field, H_{res}, and the intensity or height of the resonant absorption signal. Often, a simple linear dependence with T is observed [18-23]. Magnetic and structural phase transitions appear as a discontinuous event on this dependence [24].

The resonance field behavior with temperature for bulk and MNP's decreases with decreasing temperature, as a consequence of the enhancement of the contributions to the internal field associated with magnetic ordering (mainly exchange and anisotropy). This effect is stronger for small particles (figure 1) [25], revealing additional contributions to the internal field at low temperatures as a consequence of the size decreasing. These contributions can be assumed as an extra unidirectional internal field arising from surface disorder, where the magnetization processes are presumably to be isotropic and causes an extra shift of the resonance field. Therefore, as the surface area increases with decreasing the particle size, the isotropic effects on the magnetic resonance behavior are more pronounced and an additional distribution of energy barriers, promoted by surface isotropic disorder, must be assumed.

As observed in many works [23,25-27], the FMR spectra for MNPs at intermediate temperatures results to be a mixing of two lines: a broad component corresponding to typical anisotropic contributions and a narrow one, presumably corresponding to the surface isotropic contributions. This leads to a characteristic FMR shape for nanoparticulated systems. The general features include a broad component (becoming wider and shifting to lower fields upon cooling, see figure 2), a narrow component, and a large broadening and shifting as the particle size decreases. Figure 2 shows the FMR signal evolution with temperature variation from room temperature down to 100 K for a well diluted magnetite suspension [26]. A double component spectrum is well observed at high temperatures, while its two components seem to overlap in a single broad signal as temperature goes down. This can be attributed to an important decrease on isotropic

contributions which causes the narrow component to disappear at low temperatures. In addition, decreasing temperature makes the broad component to widen, becoming more symmetric, and shifting to lower fields, thus revealing a random distribution of the anisotropy axis enhanced at low temperatures. Inter-particle interactions are negligible and do not contribute to this broadening since the high dilution of the studied suspension promotes isolation between particles.

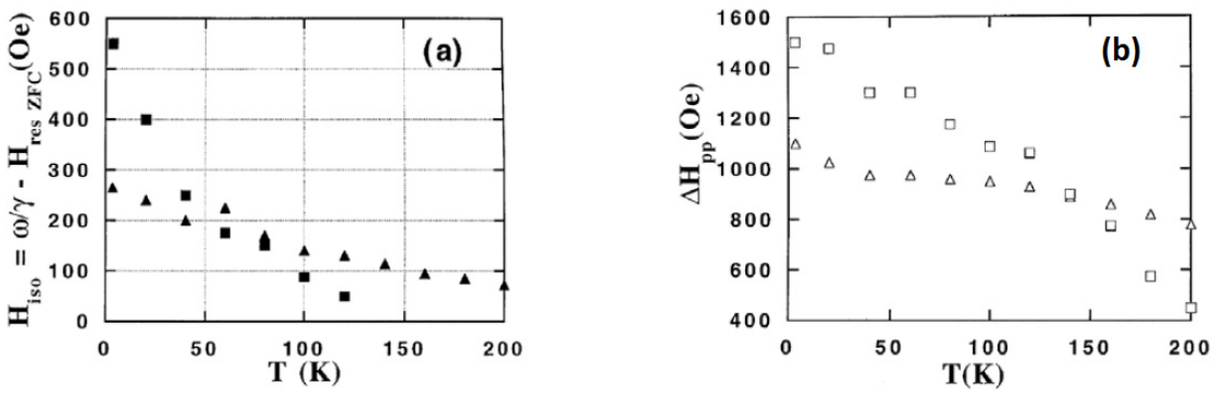

Figure 1. (a) Isotropic shift from the reference field (H_{res}=3.3 kOe) as a function of temperature for ZFC non-interacting maghemite (γ-Fe2O3) nanoparticle ferrofluid samples: (■) d = 4.8 nm (▲) d = 10 nm. (b) Peak to peak linewidth ΔH_{pp} as a function of temperature for ZFC non-interacting maghemite (γ-Fe2O3) nanoparticle ferrofluid samples: (□) d = 4.8 nm (Δ) d = 10 nm [25].

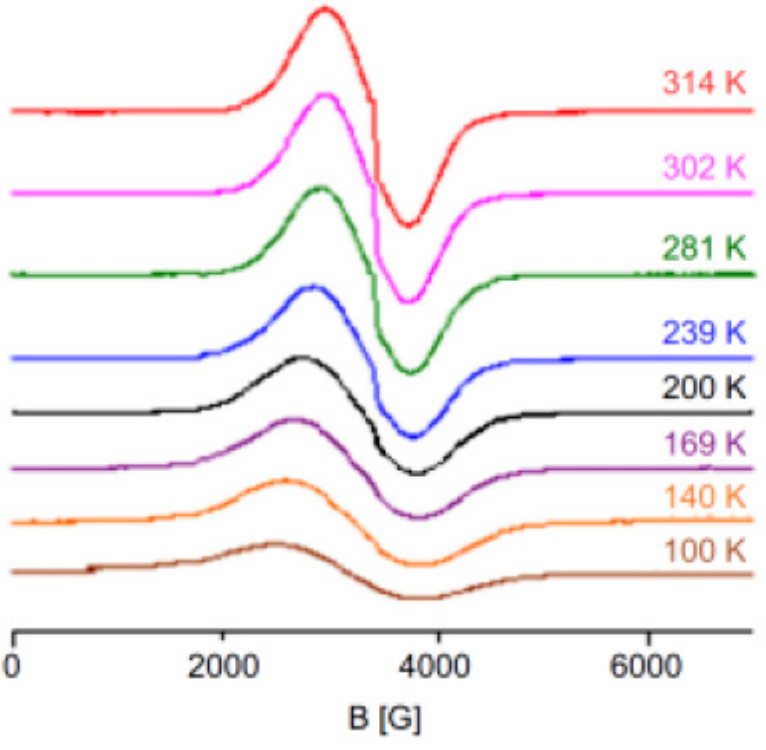

Figure 2. FMR signal evolution with temperature for a 0.1 wt% polymer Fe_3O_4 suspension [26].

Figure 3 shows the absorption signals for different particle distribution sizes of non-interacting maghemite (γ-Fe_2O_3) nanoparticle ferrofluid samples at room temperature [27]. The absorption signal changes drastically with changes on the particle size. Two limit cases are observed. The upper limit, for the largest size particles (sample 2, d = 10 nm), corresponds to a wide line shifted to a lower field in comparison with the reference (ω/γ = 3.3 kOe, where γ is the gyromagnetic ratio for free electrons). This line seems to be characteristic for anisotropic contributions. On the contrary, for the smaller size particles (sample 6, d = 10 nm) the spectrum shows a much narrower line, apparently characteristic for isotropic contributions and not shifted from the reference. The FMR signals for intermediate cases result in a more complex double-feature shape spectrum (samples 3, 4 and 5). Such behavior may be explained in terms of a mixing of two overlapped signals, the broad anisotropic shifted line and the narrower one, isotropic and not shifted. The coexistence of these two different contributions reveals the presence of a core-shell structure for the studied nanoparticles.

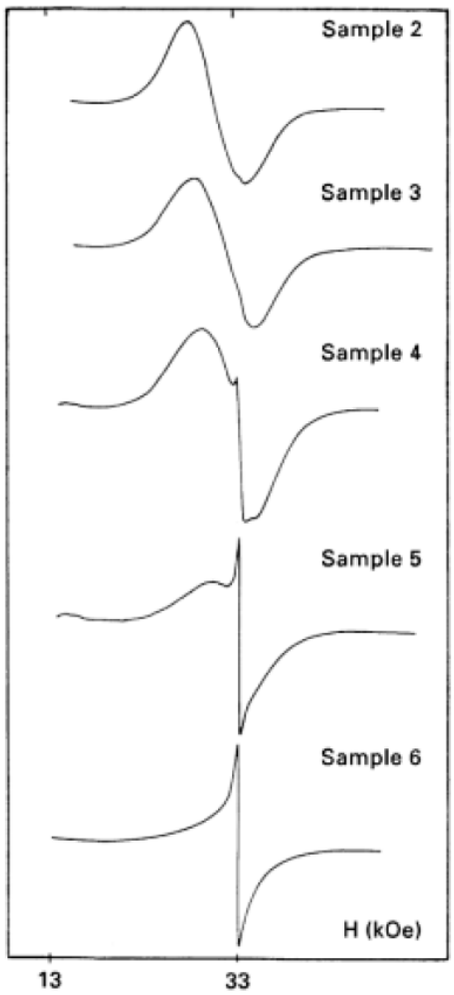

Figure 3. Influence of the particle size on X-band FMR spectra measured at room temperature for ZFC non-interacting maghemite (γ-Fe_2O3) nanoparticle ferrofluid samples. The particle size decreases from sample 2 to 6; sample 2 has the largest particle size distribution (d = 10 nm) and sample 6 the smaller particle size distribution (d = 4.8 nm) [27].

Particle concentration dependence

Double component FMR spectra have also been reported for solid and liquid Fe_3O_4 suspensions [26]. Important changes were observed on the absorption signal depending on the particle concentration. Figure 4 shows the decrease of the narrow component as the concentration increases. Both components exhibit also a broadening as the concentration increases. This important dependence of the signal linewidth with concentration is due to an increase of particle dipolar interactions at mean distances and a consequence of aggregation [28-30].

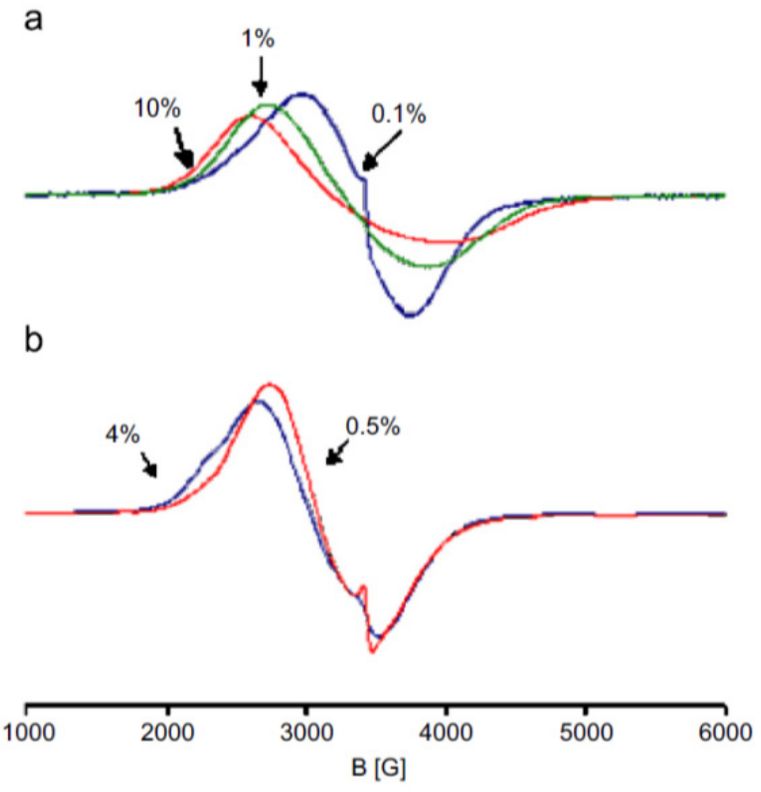

Figure 4. FMR signals for solid (a) and liquid (b) Fe_3O_4 suspensions at different concentrations [26].

Particle interactions always play an important role on the magnetic resonance absorption phenomena. FMR at different frequencies on dispersed KBr and then compressed $NiFe_2O_4$ commercial nanoparticles has recently been reported [31]. The resulting pellets showed strong shape anisotropy, as in-plane and out-of-plane analyzed measurements diverge with the increase of nanoparticle packing fraction (figure 5).

The resonance field decreases with increasing volume for in-plane measurements. In contrast, for out-of-plane measurements it increases with volume fraction. Both cases (in and out of plane), showed a resonance field shifted to a lower field in comparison with an ideal bulk as reported. As the packing fraction decreases, the in-plane and the out-of-plane curves converge to the same field value (≈ 0.04 T). This value can be identified as the average effective anisotropy field of the particles. A useful and powerful tool to estimate particle anisotropy can be based on these measurements.

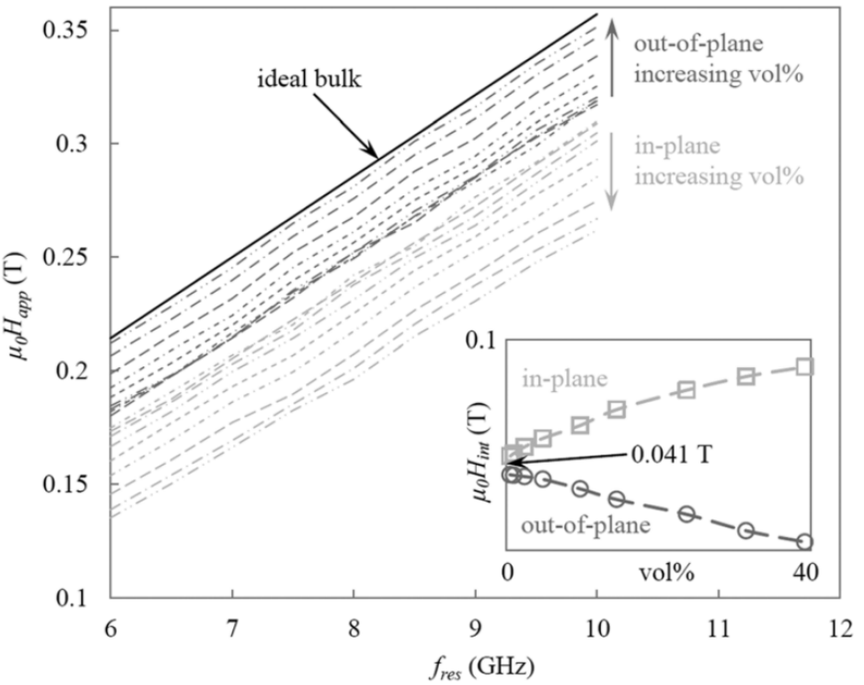

Figure 5. Frequency and shape orientation dependence of the applied field, at which FMR occurs, for commercial $NiFe_2O_4$ nanoparticles, dispersed in KBr and then compressed with different packing volume fractions. The inset shows the evolution of the resonance field as a function of the packing volume fraction [31].

Angular dependence

The anisotropy distributions and its FMR signal effects on MNP's can be carried out by measuring the angle variation between the cooling field of field-cooled (FC) samples. By comparing the obtained spectra for different orientations of FC samples, it is possible to determine the contribution of the anisotropy distribution within each particle to the FMR signal. The corresponding resonance lines often lead to a double component signal. It is then possible to separate the contributions which have a strong dependence with the angle from the weakly dependent counterpart. The narrow component can be attributed to surface anisotropy, while the the broad component should be associated with internal anisotropy of the NPs. Recent works have demonstrated the isotropic/anisotropic nature of most common MNP's, as described above. Figure 6 shows differences between FMR spectra for parallel and perpendicular configurations of FC samples. The samples consisted of maghemite nanoparticles with a particle diameter reported as 4.8 nm [27]. At the high temperature (top in figure 6), no variation as a function of θ is observed for the narrow component, while the broad component, on the contrary, shifts to higher resonance fields as the angle θ increases (bottom in figure 6). The narrow component is not affected by angular variations.

The resonance field of the anisotropic component generally is plotted against the angle θ, the dependences with θ use to be fitted, in good agreement, with $\sin^2 \theta$ or $\cos^2 \theta$ functions [24-32]. Its well established the axial symmetry nature for this kind of functions, as magnetization processes perform the higher energy absorption (energy improved by the resonance field) when the magnetizing field is perpendicular to the axial orientation, the

resonance field also increases and finds a maximum at this position. The differences between the resonance field at θ = 0° and θ = 90°, are related to the anisotropy field, promoted by the respective axial anisotropy within the core of the nanoparticles revealing a mono-domain configuration on this region (figure 7).

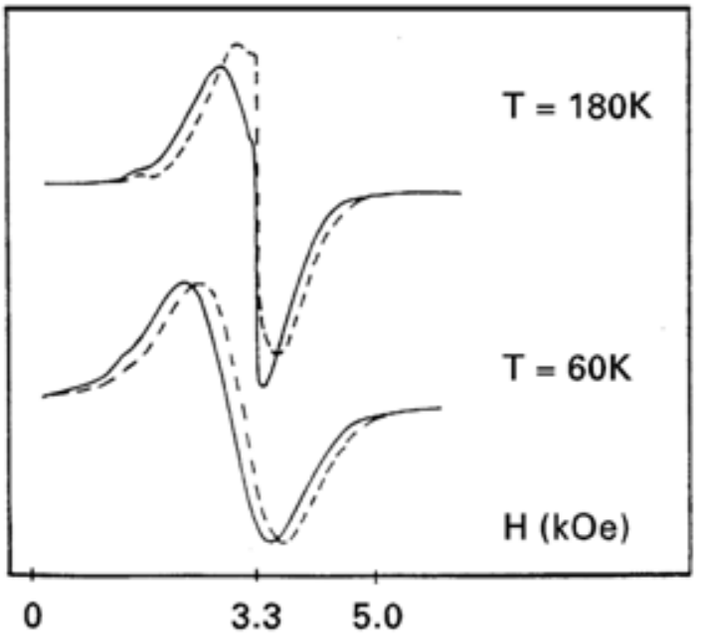

Figure 6. X-band FMR spectra of maghemite FC nanoparticles dispersed on glycerol, with a 10 kOe cooling field. Solid and dashed lines correspond respectively, to configurations with the scanning field parallel (θ = 0°) and perpendicular (θ = 90°) to the cooling field [27].

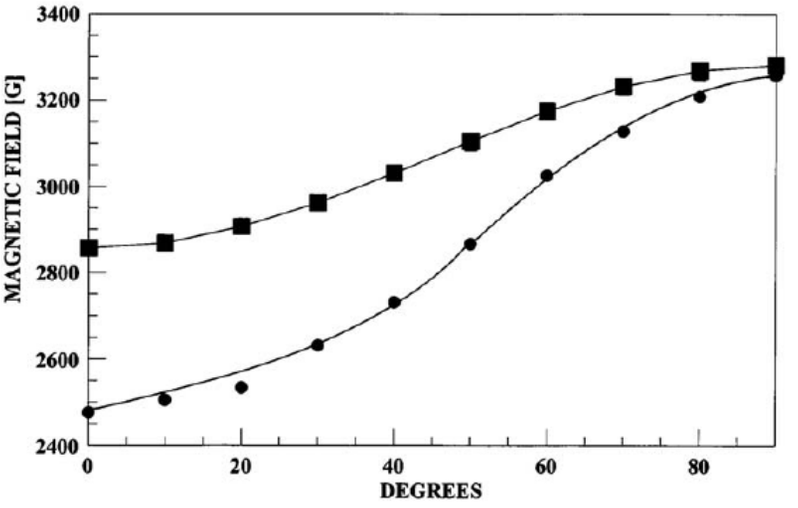

Figure 7. Dependence of the resonance field with θ for field-cooled (FC) hematite NPs at 300 and 155 K (lower curve) [24].

The fitting of the angular resonance field dependence is useful to determine anisotropy parameters. The dependence can be given by [32]:

$$H_r = H_o - H_a(1/2)(3cos^2\theta - 1) \quad (1)$$

where H_r is the resonance field, $H_a = 4|K|/M$ is the anisotropy field (with $|K|$ the absolute value of the anisotropy constant and M the magnetization), and H_o measures the g value. The g value is a constant describing the relation between the energy of the microwave radiation and the *dc* magnetic field. For the parallel configuration the resonance field is:

$$Hr = Ho - 4|K|/M \tag{2}$$

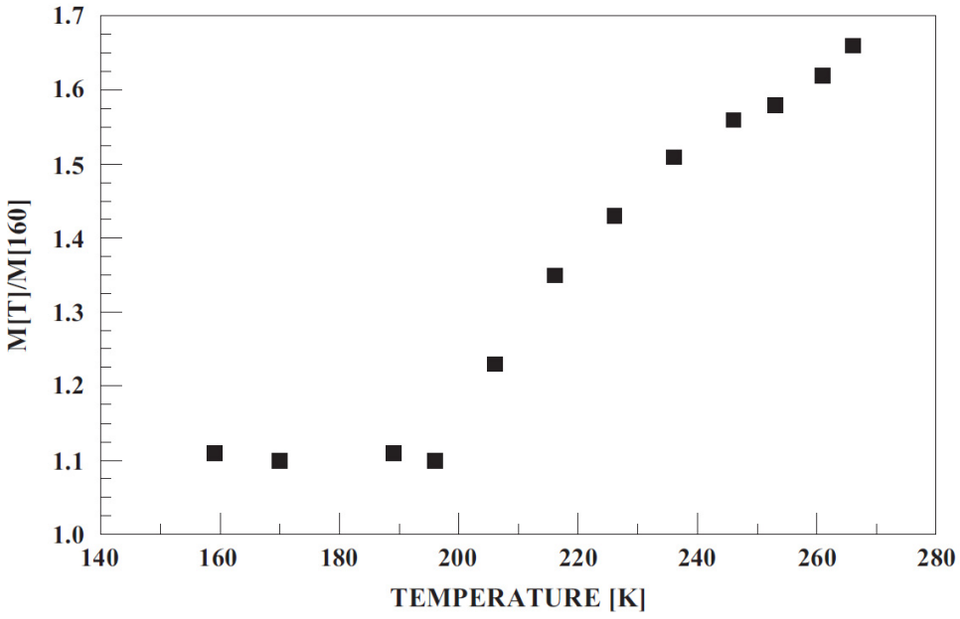

Figure 8. Reduced magnetization dependence with temperature for a FC hematite NPs [24].

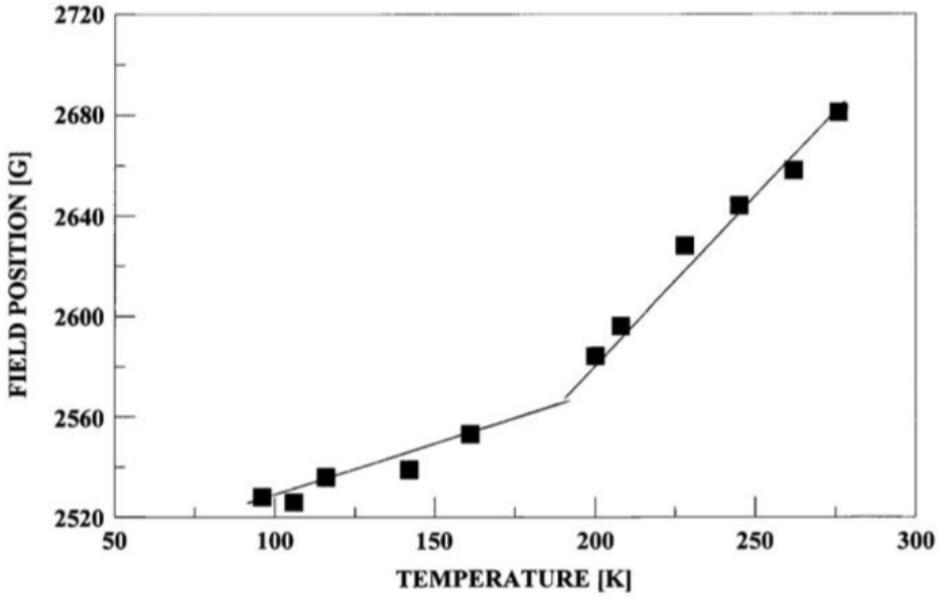

Figure 9. Resonance field dependence with temperature for hematite sample of Fig. 8 [24].

Magnetic phase transitions produce significant changes in $|K|/M$ and hence on the resonance field. The parallel configuration can therefore be used to investigate phase transitions.

Figure 8 shows the temperature dependence of magnetization of FC hematite NPs, parallel to the cooling field [24]. A change in the slope is observed in good agreement with observed transitions from a disordered phase to a magnetically ordered phase. In contrast with bulk hematite (antiferromagnetic above 260 K), these hematite NPs exhibited a superparamagnetic behavior, which can be explained in terms of a weakly ferromagnet below ~ 200 K, as shown in figure 8. The reported transition is also observed in plots of the resonance field against temperature (figure 9) and other FMR spectrum parameters, which suggest the FMR technique as a useful tool to investigate phase transitions on MNP's.

Effects of the aggregation state

Ferrite NPs can show the effects of two extreme aggregation states, namely monodisperse NPs, and clusters of a few hundreds of NPs. Samples of composition $Zn_{0.5}Ni_{0.5}Fe_2O_4$ were prepared by the polyol method, and designated as "A" for monodisperse state, and "B" for clusters. FMR spectra exhibited significant differences, as shown in Fig. 10. The decrease in the effects of surface for sample B appear in the form of a lower resonance field and an increase in the linewidth, as compared with sample A. The former can be understood in terms of a larger internal field in the cluster sample as a consequence of the aggregation of NPs; simply, the NPs inside the cluster tend to behave as grains in a bulk material. The effects of surface (crystal defects, unsatisfied bonds, etc.) are relieved by the presence of other NPs. Magnetic exchange interactions among neighboring NPs can also be assumed, which increases the internal field and thereby decreases the applied magnetic field needed to fulfill the Larmor equation conditions. On the other hand, these interactions increase the linewidth, especially the random distribution of anisotropy axes.

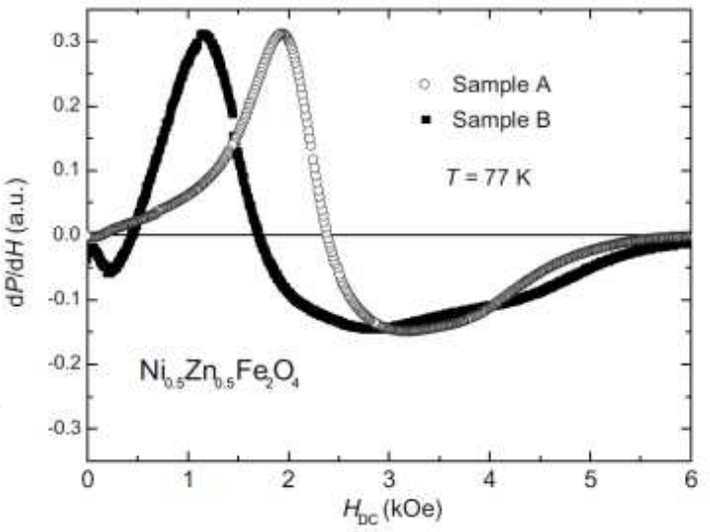

Figure 10. FMR spectra of Ni-Zn ferrites at 77 K, in monodisperse state (Sample A), and clusters (sample B) [18].

At room temperature, as shown in Fig. 11, isolated NPs show a superparamagnetic phase and again a larger resonance field with a significant reduction in linewidth as the factors just mentioned, associated with an ordered magnetic structure, are absent. The cluster sample exhibits a reduced linewidth, but always larger than the superparamagnetic state.

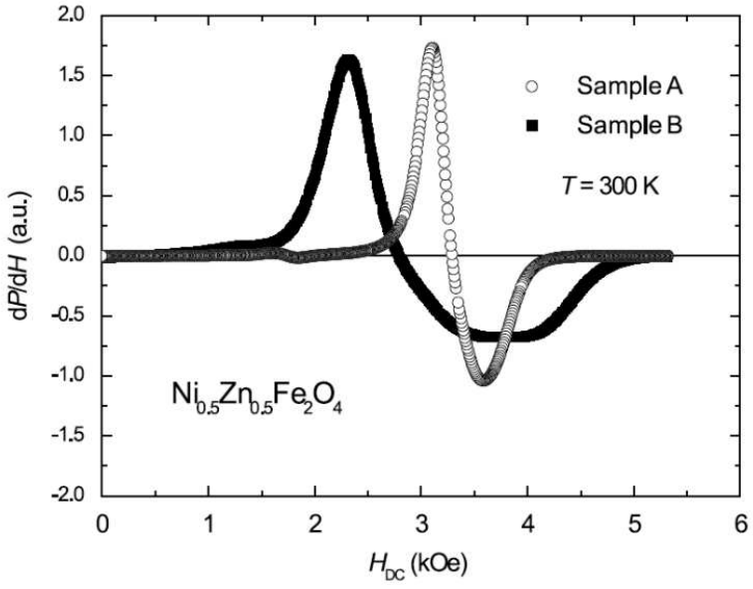

Figure 11. FMR spectra of Ni-Zn ferrites at 300 K, in monodisperse state (Sample A), and clusters (sample B) [18].

3. Ferromagnetic resonance in nanostructured ferrites

Ferrite NPs have to be consolidated as a high density solid for many applications (in electronic devices, for instance), where a powder is unstable. Typical sintering processes needing high temperatures are difficult to apply, as NPs tend to grow very rapidly at temperatures above 500°C, losing the nanometric size range and thus the different properties associated with this size range. A particularly well suited method to consolidate NPs into a high density nanostructured solid preserving grains within the nanometric range is Spark Plasma Sintering (SPS for short) [33]. Also known as pulsed electric current sintering (PECS), in this technique the sample (typically in the form of a powder) is placed in a graphite die and pressed by two punches at pressures in the 200 MPa range, while a strong electric current goes through the system; the die is shown in Fig. 12. SPS therefore consolidates powders under the simultaneous action of pressure and electric current pulses (typically of a few milliseconds in duration [33]).

The electric current pulses result in a very rapid heating of the sample, at rates as high as 1000°C/min. If the sample is a good conductor, current goes through it and the heating is even more efficient. A significant point is that the electric current has a significant impact on the atomic diffusion during the process [34]. The sintering process can then reach high densities at very low temperatures and extremely short times [35]. Obviously, SPS can also be utilized for reactive sintering involving a chemical reaction [36].

SPS has been used to consolidate spinel [37], garnet [38], and hexagonal ferrites [39]. In the case of spinel $Ni_{0.5}Zn_{0.5}Fe_2O_4$ ferrites, samples prepared in the form of 6-8 nm nanoparticles by the forced hydrolysis in a polyol method [12], were consolidated by SPS at temperatures in the 350-500°C range by times as short as 5 min. Just for comparison, the typical conditions for sintering in the classic solid state reaction are 1200°C for at least 4 hours. NPs growth

was controlled, as the final grain size in the consolidated ferrite was about 60 nm, even for the highest (500°C) SPS temperature [40].The densities reached values as high as 94% of the theoretical value. FMR spectra obtained at 77 and 300 K are shown in Fig 13, together with the FMR signal corresponding to the original NPs. The resonance field exhibited a decrease as the SPS temperature increased, which can be explained in terms of the components of the total field in the Larmor expression, $\omega = \gamma H$. The main components of the total field are $H = H_{DC} + H_X + H_a + \ldots$, where H_{DC} is the applied field, H_X is the exchange field responsible for magnetic ordering, and H_a is the anisotropy field. As magnetic ordering sets in, H_X and H_a increase and therefore the applied field is decreased in order to fulfill the Larmor resonance conditions. As sintering progresses, the surface effects decrease and the material has the tendency to behave as a bulk ferrite.

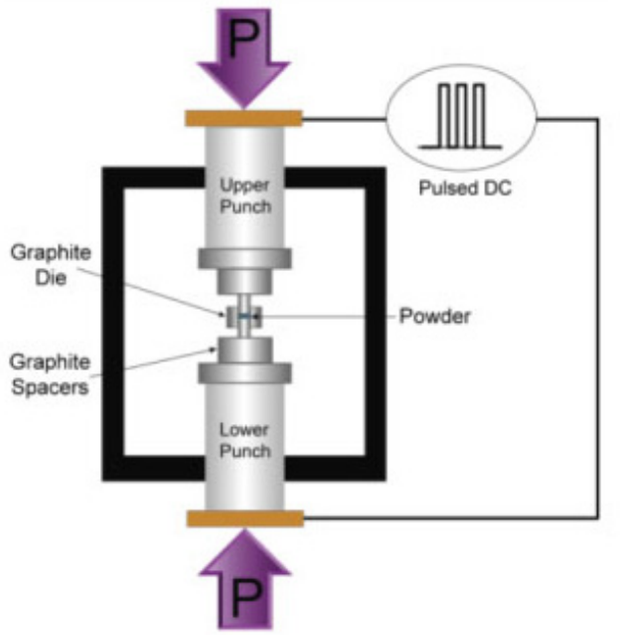

Figure 12. Schematic of spark plasma sintering apparatus [33].

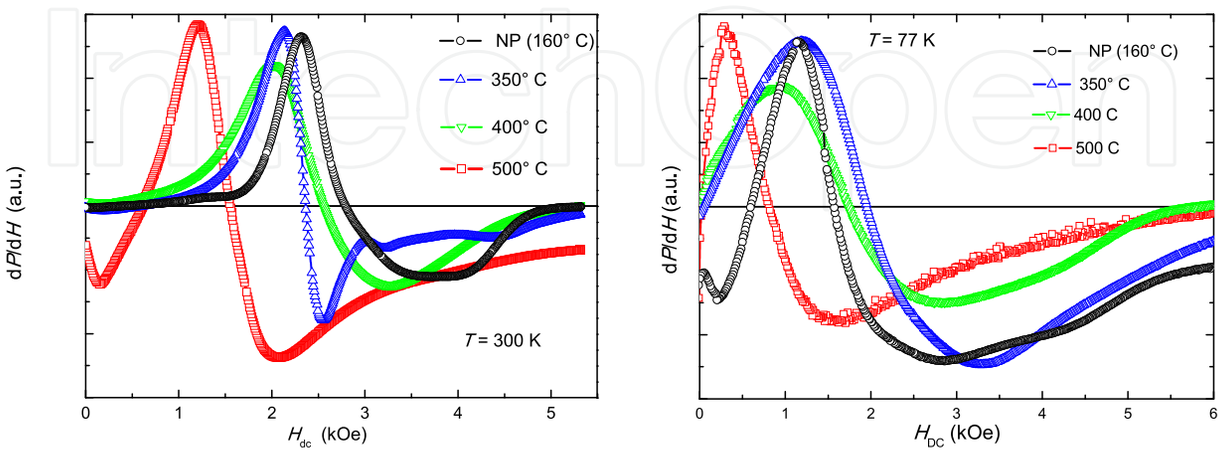

Figure 13. Ferromagnetic resonance of Ni-Zn ferrites prepared by a chimie douce method followed by SPS at temperatures in the 350-500°C range for 5 min. The FMR response of the original NPs is also shown for comparison. (Adapted from [40]).

All the samples exhibited a large broadening in the linewidth, generally interpreted by considering a random distribution of the anisotropy axis in single domain NPs [41]. The broadening decreases as consolidation increases, as the surface effects are diminished by formation of grain boundaries. At room temperature the linewidth decreases since all the samples approach the paramagnetic state where the internal field is eliminated and only the applied field is involved in the Larmor expression. The NPs signal exhibited the lowest linewidth as at room temperature these NPs are superparamagnetic; all the consolidated samples showed a ferrimagnetic behavior at 300 K as compared with the as-produced sample which has a blocking temperature about 90 K.

4. Paramagnetic resonance in ferrite nanoparticles

Zinc ferrite is a very good material to investigate the site occupancy by cations. In spite of a relatively large cation radius, Zn^{+2} has a tendency to occupy tetrahedral sites, while Fe^{3+} fill octahedral sites [1], in other words, a "normal" spinel. This arrangement leads to B-O-B superexchange interactions between iron cations and therefore to an antiferromagnetic structure with a Néel temperature about 9 K. In the case of nanosized Zn ferrite, however, the cation distribution can be significantly different; some degree of inversion occurs [1,42], with a fraction of Zn^{2+} on octahedral sites, and hence Fe^{3+} on both sites. The spinel becomes ferromagnetic, with a Curie temperature well above 9 K.

The variations in linewidth, ΔB_{PP}, and g-factor, g_{eff} in these ferrites depend mainly on the interparticle magnetic dipole–dipole interactions and intraparticle super-exchange interactions. On the other hand, the interparticle superexchange between magnetic ions (through oxygen) can reduce the value of linewidth. The magnitude of this interaction is determined by the relative position of metallic and oxygen ions. When the distance between the metallic and oxygen ions is short, the metal cations have an exactly half-filled orbital, and the angle between these two bonds is close to 180°, the superexchange interaction is the strongest [43].

Several factors can produce a distribution of local field, such as unresolved hyperfine structure, g-value anisotropy, strain distribution, crystal defects. The field strength on a particular spin is then modulated by local field distribution and leads to an additional linewidth broadening [44,45].

The strain distribution produced by a small average particle size can cause a small resonance signal [1]. As the particle size is increased, such small signal disappears and only the broad signal remains. This suggests that the particle size has a threshold value above which the strains are relieved.

In order to gain some insight into the relationship between internal structure and EPR spectra, it can be useful to compare the properties of several iron-based oxide NPs embedded in a polytethylene matrix, prepared by the same method: Fe_2O_3, $BaFe_2O_4$, and $BaFe_{12}O_{19}$ [46]. The experimental EPR spectra of the samples are presented in Figs. (14-20). At room temperature the EPR spectra of all the samples show a ''two-line pattern'' (Fig. 14)

which is typical of superparamagnetic resonance (SPR) spectra. The relative intensity of these lines depends on the particle size and shape distribution function [47]. For the Fe_2O_3 and $BaFe_2O_4$ samples, the broad line predominates in the room temperature spectra; the opposite is observed for the $BaFe_{12}O_{19}$ sample, where the narrow line is more pronounced.

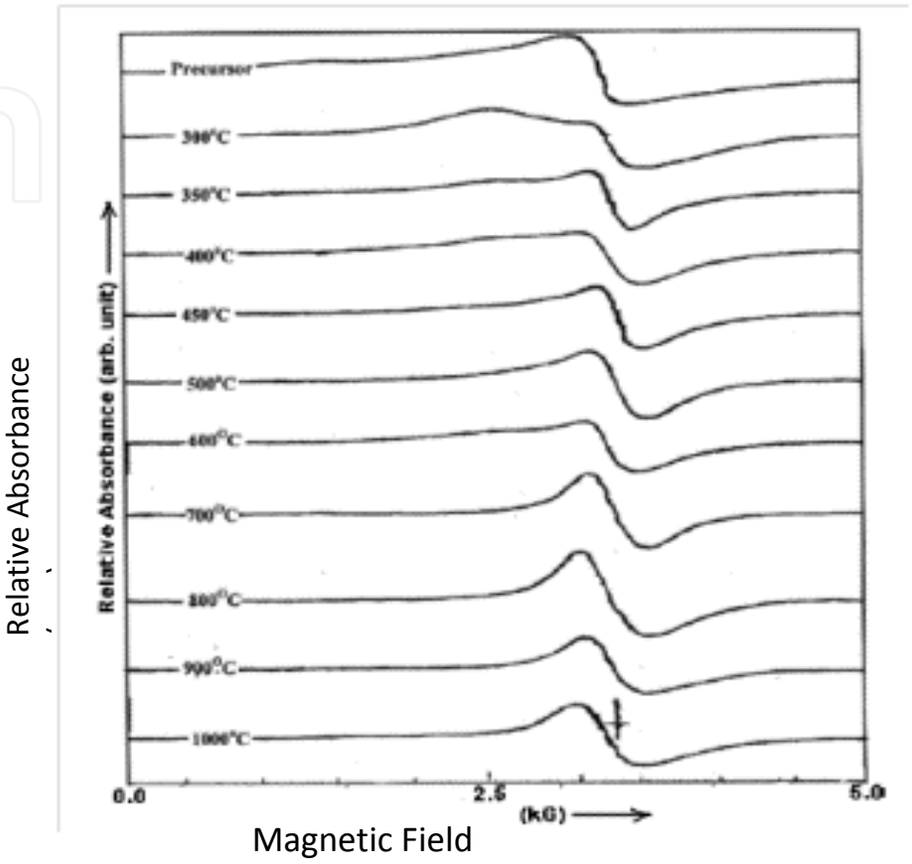

Figure 14. EPR spectra of zinc ferrite sintered at different temperatures.

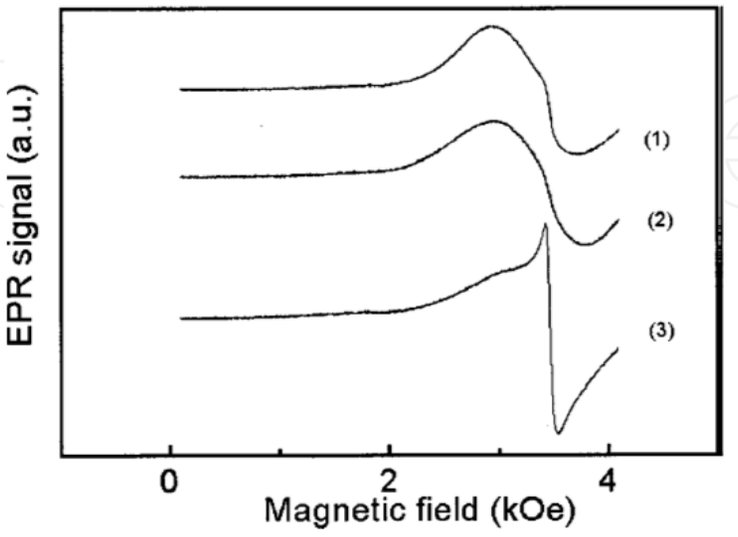

Figure 15. Room temperature EPR spectra of nanoparticles: Fe_2O_3 (curve1), $BaFe_2O_4$ (curve 2), and $BaFe_{12}O_{19}$ (curve3) [46].

At room temperature, the spectra of all samples show a "two-line pattern" (Figure 15) which is typical of superparamagnetic resonance. These spectra can be considered as a broader line superimposed on a narrow line. The relative intensity of these lines depends on the particle size and shape distribution function, as well as on the magnitude of the magnetic anisotropy. For Fe_2O_3 and $BaFe_2O_4$ samples, the broad line predominates in the RT spectra. This line is characterized by a peak-to-peak linewidth of ΔH ~ 850 Oe and an effective g-value of 2.07. In the RT spectrum of $BaFe_{12}O_{19}$ sample, in contrast, the narrow line is more visible, with ΔH ~ 120 Oe and g ~ 2.0.

At low temperatures, the EPR spectra of Fe_2O_3 change significantly (Fig.16). On cooling below 100 K, the broad line S1 shows a monotonous increase of the linewidth ΔH and a decrease of the amplitude A. However, below about 50 K new resonances, S2 and S3, appear in the spectra of Fe_2O_3 (Figs. 16 and 17). It is interesting that S2 behaves like a typical paramagnetic resonance signal, namely, the amplitude increases and the linewidth decreases as the temperature is diminished. The EPR spectra suggest that Fe_2O_3 nanoparticles contain both ferromagnetic and antiferromagnetic phases. The weak EPR signal of the rhombic symmetry ($g \approx 4.3$) that appears at low temperatures may be attributable to an α-Fe_2O_3 phase that undergoes an antiferromagnetic-like transition near 6 K. [46]

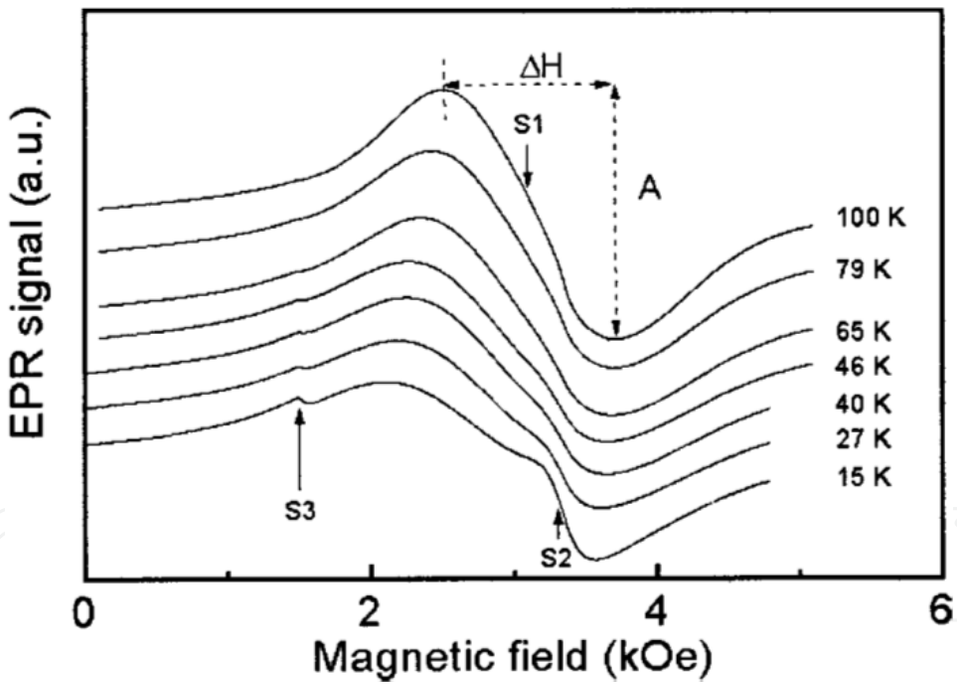

Figure 16. EPR spectra of Fe_2O_3 nanoparticles at different temperatures. [46]

EPR spectra of the $BaFe_2O_4$ nanoparticles at different temperatures are shown in Fig. 18. At all temperatures the spectra are broad and rather asymmetric. A significant shift of the line position to low magnetic fields and a marked spectrum broadening are observed at low temperatures.

On the other hand, the thermal variations of EPR spectra of the $BaFe_{12}O_{19}$ sample is typical of superparamagnetic resonance. The relatively narrow line that dominates at room

temperature disappears as temperature decreases (Figs. 19 and 20). The $BaFe_{12}O_{19}$ nanoparticles reveal an EPR signal that is significantly narrowed at high temperatures by superparamagnetic fluctuations. This is evidence of the reduced magnetic anisotropy energy that may be due to the particle's nanosize (effective diameter <10 nm).

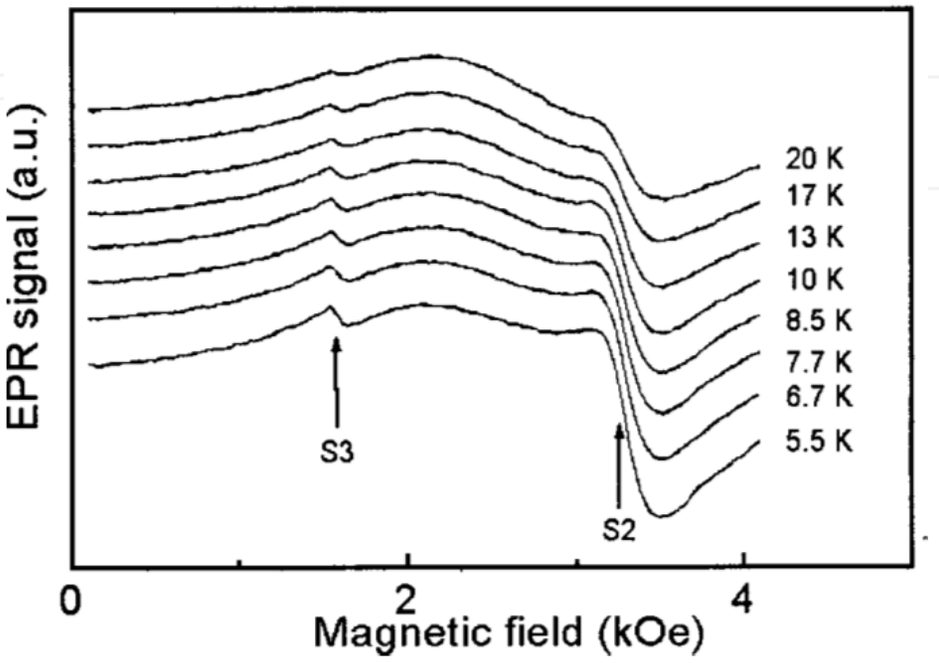

Figure 17. EPR spectra of Fe_2O_3 nanoparticles at low temperatures. [46]

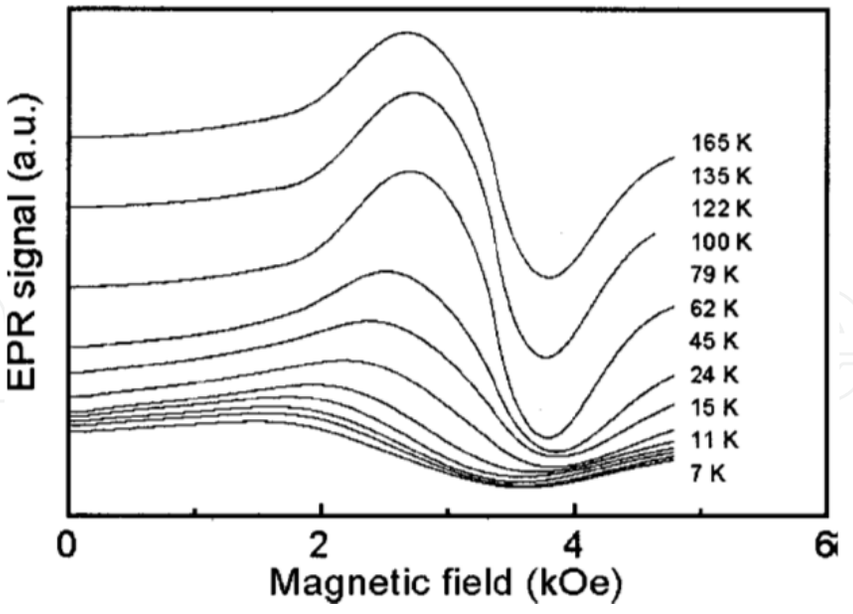

Figure 18. EPR spectra of the $BaFe_2O_4$ nanoparticles at different temperatures. [46]

These results show that EPR spectra at low temperatures are desirable for the correct identification of NPs and a comparison with high temperature experiments allows a better understanding of phenomena related with variations associated with nanosized materials.

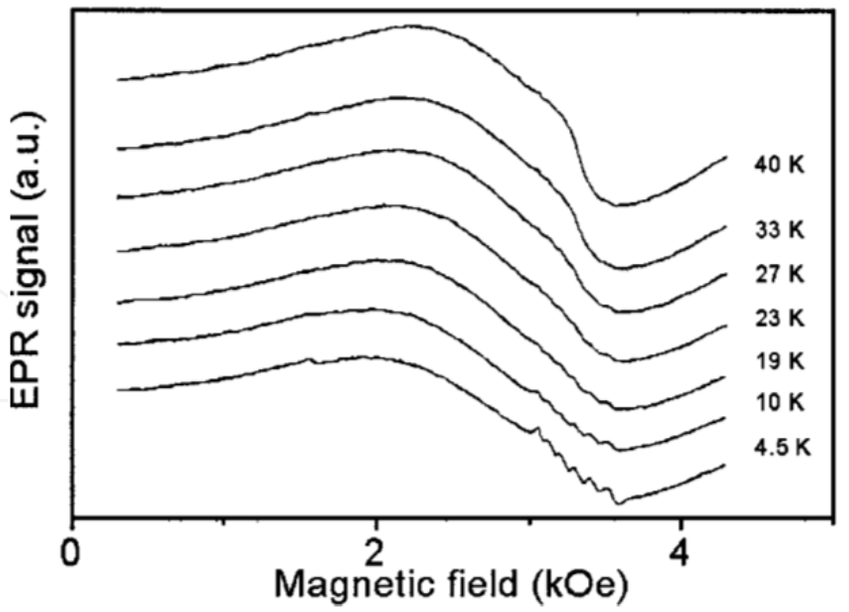

Figure 19. Low-temperature EPR spectra of $BaFe_{12}O_{19}$ nanoparticles. [46]

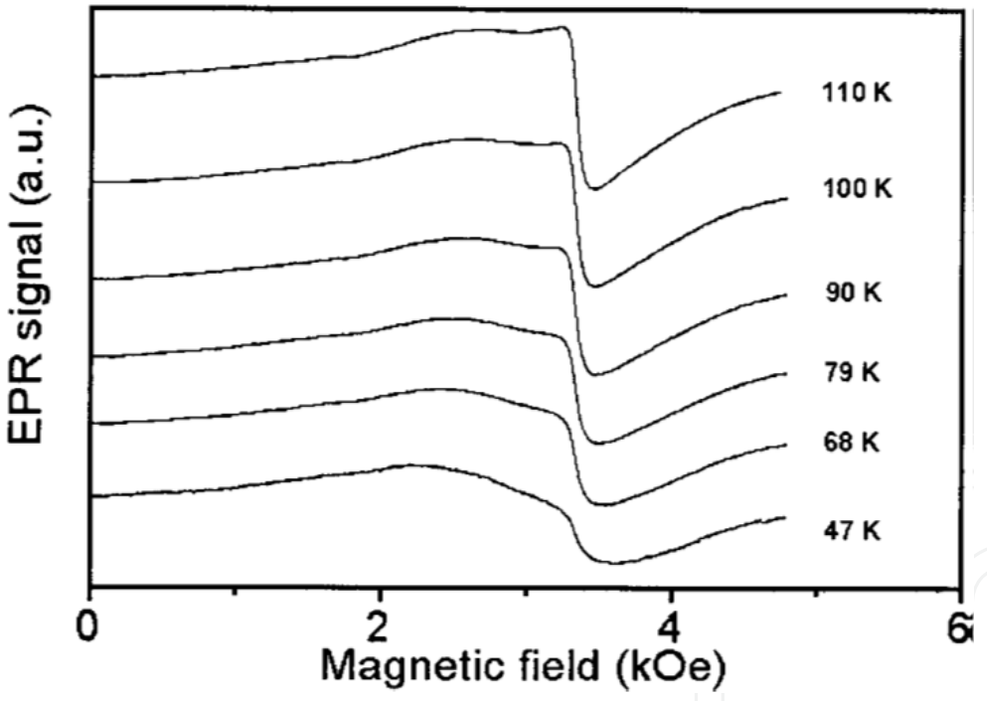

Figure 20. EPR spectra of $BaFe_{12}O_{19}$ nanoparticles at different temperatures. [46]

5. Low Field Microwave Absorption (LFMA)

Low field microwave absorption (LFMA for short) refers to the non-resonant, hysteretical losses of a material subjected to a high frequency electromagnetic field. Recently, it has become a useful method to investigate magnetization processes [48], magnetoelastic effects [49], phase transitions [50], non-aligned ferromagnetic resonance [51,52], spin arrangements [53,54]. LFMA is similar to giant magnetoimpedance (GMI) [55], but physically different to

ferromagnetic resonance (FMR) [56]). GMI, generally defined as the variations of impedance of a magnetic conductor carrying an alternate electrical current when subjected to an external magnetic field [57], extends into a very wide frequency range. Clearly, GMI is a non-resonant phenomenon as confirmed by two facts: GMI does not fulfill the resonant Larmor conditions, and exhibits magnetic hysteresis.

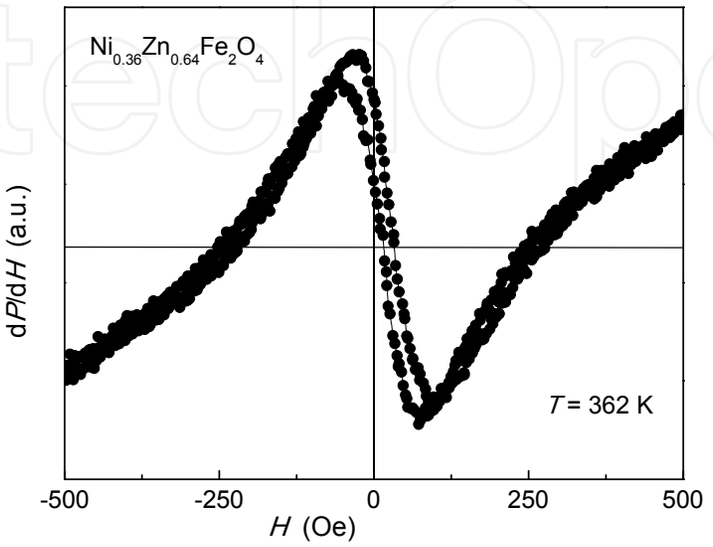

Figure 21. Typical "positive" LFMA signal from a Ni-Zn bulk ferrite (Adapted from [59]).

LFMA is associated with magnetization processes in magnetically ordered materials, in the process from the unmagnetized state to the magnetic saturation. In bulk ferro and ferrimagnetic materials, LFMA exhibits a flat response in the paramagnetic phase. To measure experimentally LFMA in a typical FMR/EPR facility, the applied field has to be cycled; usually between -1 kOe and +1kOe is enough. Also, a device to compensate for the remanent magnetization is needed in most electromagnets.

An important parameter is, of course, the total anisotropy field of the particular sample. In most cases, LFMA exhibits a critical behavior at the total anisotropy field in the form of a maximum and a minimum, leading to a characteristic signal as shown in Fig. 21 [59]. In bulk Ni-Zn ferrite, a correlation exists between the magnetocrystalline anisotropy and the half-peak-to-peak, measurement of LFMA. Figure 22 shows a comparison between the peak-to-peak LFMA field (divided by 2) [60] and a calculation from magnetocrystalline constant, K_1,published results [61]. The small differences can be attributed to shape anisotropy, as the calculation is based solely on K_1.

LFMA seems to be associated with spin structure. By convention, this signal can be assigned as "positive", simply because it has the same shape than the FMR/EPR signal, i.e., a maximum and a minimum when observed from left to right. A positive LFMA sign has been observed in most insulator and semiconductor materials, while a "negative" signal appears for most metallic conductors, as shown in Fig. 23, for a Co-rich CoFeBSi amorphous microwire [59]. An interesting result was found in bulk Ni-Zn ferrites showing the Yafet-Kittel triangular arrangement [62], by measuring the LFMA as a function of temperature in

the 150 K-240K temperature range [63]. The LFMA sign changed from negative at ~ 154 K to positive at $T \geq 240$ K.

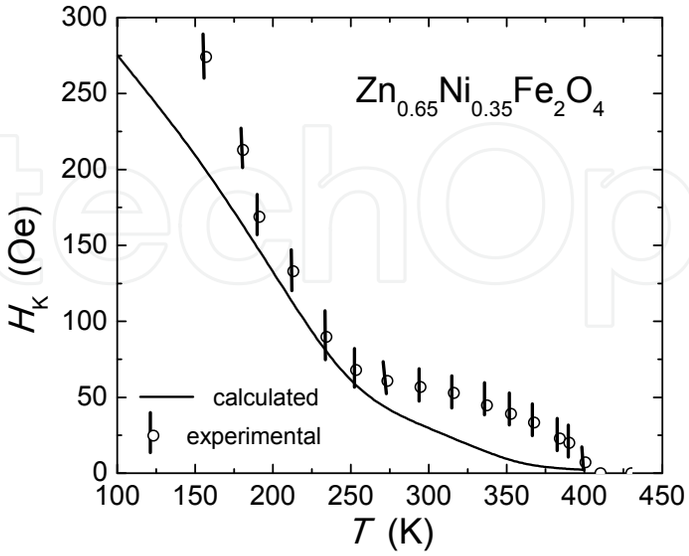

Figure 22. Fig. 21. Correlation between the field on LFMA critical points (divided by 2) and a direct calculation of magnetocrystalline anisotropy in $Zn_{0.65}Ni_{0.35}Fe_2O_4$ bulk ferrites [60]. K_1 anisotropy constant data for the calculation was obtained from ref [61].

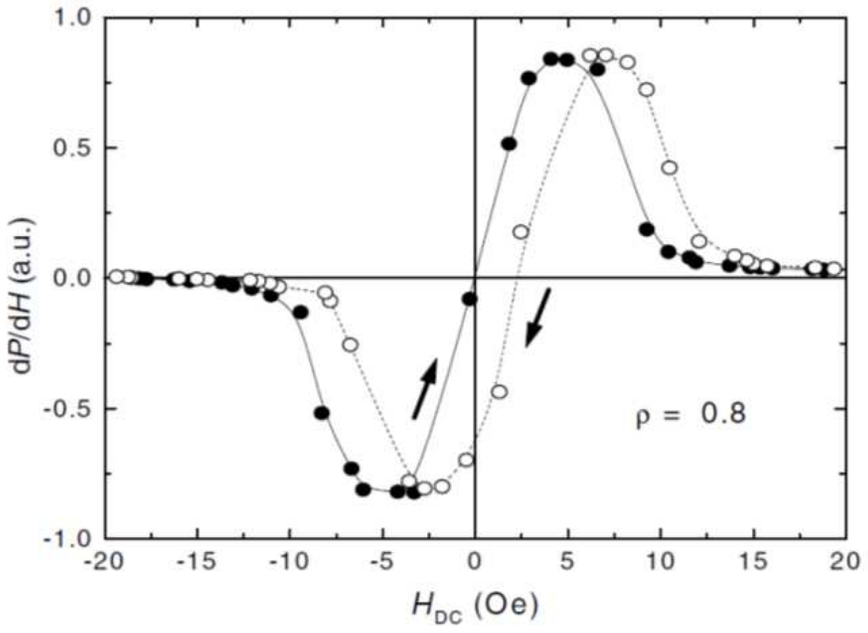

Figure 23. LFMA from a Co-rich CoFeBSi glass-covered amorphous microwire [59]. This is an example of a "negative" LFMA signal, mostly observed in conductor materials (compare with Fig. W above).

LFMA in NPs

LFMA can provide useful insights into the structure of NPs. When two different aggregation states are compared, i.e., monodisperse and clustered NPs with the same composition and NP diameter, clearly different spectra are obtained. By varying the synthesis conditions in

the forced hydrolysis in a polyol method [12], Ni-Zn ferrites can be obtained as monodisperse, well crystallized ~ 6 nm NPs on one hand, and labeled as sample "A"; on the other, clusters about ~ 100 NPs constituted by NPs with the same composition and diameter [58], labeled as sample "B". It is interesting to mention that high resolution transmission electron microscopy (HRTEM) showed some epitaxial arrangements within the clusters of sample B.

Sample A showed a superparamagnetic behavior at room temperature, and a blocking temperature about 50 K [58]. Sample B, in contrast, exhibited a ferromagnetic behavior up to 300 K (blocking temperature > 300 K), in spite of being constituted by NPs of the same composition and NP diameter. Clusters effectively decrease the effects of surface producing samples with a general behavior between that of NPs and bulk materials.

Figure 24 shows the LFMA signal from sample A at 77 and 300 K. AT the low temperature, a positive LFMA behavior is observed, corresponding to a non-conductor material. At 300 K, however, a flat response appears, associated with the superparamagnetic phase of these monodisperse NPs. Clearly, the superparamagnetic phase behaves like a paramagnetic signal. This flat signal with a small slope is associated with the microwave absorption of non-interacting dipoles [64].

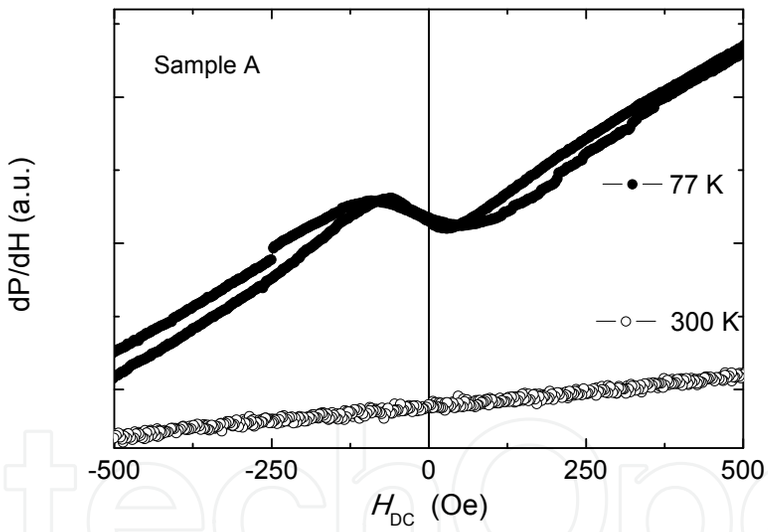

Figure 24. LFMA signal from monodisperse, ~ 6 nm diameter, $Zn_{0.5}Ni_{0.5}Fe_2O_4$ NPs, at 77 and 300 K (adapted from [58]).

Clusters of the same NPs, in contrast, showed a clear positive LFMA signal at room temperature, see Fig. 254. This is consistent, as this sample B behaved as a ferromagnetic phase close to the bulk properties.

For low temperatures, however, sample B exhibited a very different signal as shown in Fig. 26, with an important hysteresis and no similarity to either positive or negative character. As mentioned above, bulk Ni-Zn ferrites with Zn content $x > 0.5$ (in $Zn_xNi_{1-x}Fe_2O_4$) show a triangular Yafet-Kittel spin arrangement, which appears as an evolution from negative

LFMA signal at low temperatures towards a positive signal at temperatures close to room temperature [63]. Inspection of Figs. 24-26 reveals that in the case of sample A at 77 K (monodisperse NPs), no YK arrangement is manifested. Some evolution is found in sample B (clusters) at low T, but no full inversion of LFMA signal is observed. A preliminary explanation of these findings is that the surface effects inhibit the formation of the YK structure. Another possibility is based on the fact that cation distribution in NPs as synthesized by the polyol method is often different [42] as compared with bulk ferrites (prepared by the solid state reaction at high temperatures). A different cation distribution (in the present case a non-negligible concentration of Zn on B sites, for instance) could hence lead to different conditions for the formation of the YK structure.

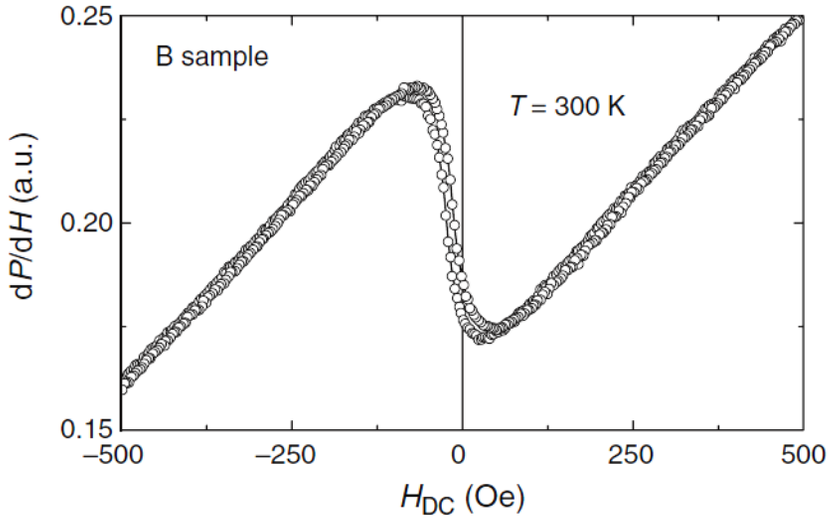

Figure 25. LFMA signal from epitaxial clusters of $Zn_{0.5}Ni_{0.5}Fe_2O_4$ ferrites, formed by a few hundreds of ~ 6 nm NPs, at 300 K.

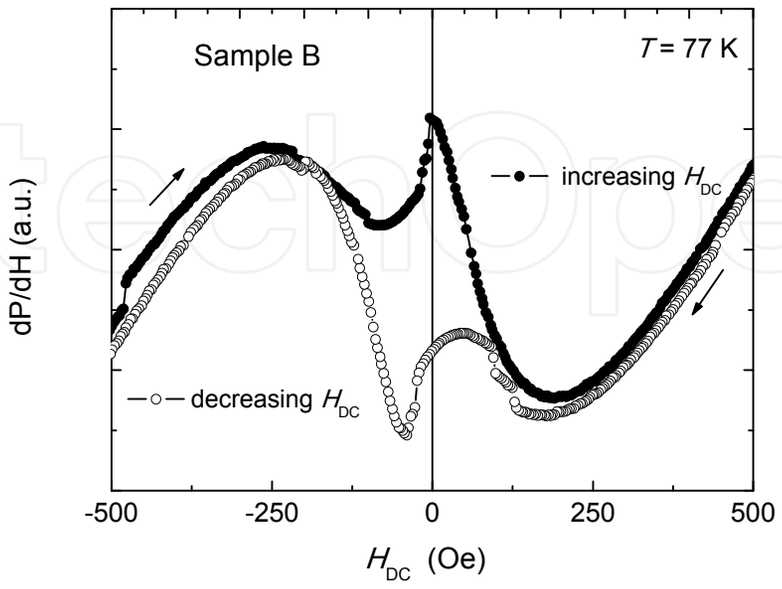

Figure 26. LFMA signal of epitaxial clusters of $Zn_{0.5}Ni_{0.5}Fe_2O_4$ ferrites, formed by a few hundreds of ~ 6 nm NPs, at 77 K.

6. Conclusions

Microwave absorption (MA) is a very sensitive phenomenon and has become an extremely powerful characterization tool. MA accurately depends on all the factors surrounding unpaired electrons; it can play a significant role in the characterization of the complex and fascinating development of magnetic nanoparticles. In this brief review, recent results on the characterization of magnetic nanoparticles and consolidated spinel ferrites by means of ferromagnetic resonance, paramagnetic resonance, and low field microwave absorption have been presented.

Author details

Gabriela Vázquez-Victorio, Ulises Acevedo-Salas and Raúl Valenzuela
Institute for Materials Research, National Autonomous University of México, México

Acknowledgement

Authors acknowledge partial support for this work from ANR-CONACyT grant 139292, as well as PAPIIT-UNAM grant IN141012.

7. References

[1] Valenzuela R. Magnetic Ceramics. Cambridge University Press (2005) (ISBN: 0-521-01843-9).
[2] Amiri S, Shokrollahi H. The role of cobalt ferrite magnetic nanoparticles in medical science. Materials Science and engineering C 2013: 33(1) 1-8.
[3] Mahmoudi M, Sant S, Wang B, Laurent S, Sen T. Superparamagnetic iron oxide nanoparticles (SPIONs): development, surface modification and applications. Advanced Drug Delivery Reviews 2011: 63(1) 24-46-
[4] Kashevsky BE, Agabekov BE, Kashevsky SB, Kekalo KA, Manina EY, Prokhorov IV, Ulashchik VS. Study of cobalt ferrite nanosuspensions for low frequency ferromagnetic hyperthermia. Particuology 2008; 6(5) 322-333.
[5] Kliza E, Strijkers GJ, Nicolay K. Multifunctional magnetic resonance imaging probes. Recent Results in Cancer Research 2013; 187 151-190.
[6] Xu Y, Wang E. Electrochemical biosensors based on magnetic micro/nanoparticles. Electrochimica Acta 2012; 84(1) 62-73.
[7] Dahawan SK, Singh K, Bakhshi AK, Ohlan A. Conducting polymer embedded with nanoferrite and titanium dioxide nanoparticles for microwave absorption. Synthetic Metals 2009, 159(21-22) 2259-2262.
[8] Liu R, Lal R. Nanoenhanced materials for reclamation of mine lands and other degrade soils: a review. Journal of Nanotechnology 2012; 461468-1-461468-18. doi: 10.1155/2012/461468.

[9] Hua M, Zhang S, Pan B, Zang W, Lv L, Zhang Q. Heavy metal removal from water/wastewater by nanosized metal oxides. Journal of Hazardous Materials 2012; 211-212 317-331.

[10] Hosokawa M, Nogi K, Naito M, Yokoyama T. Nanoparticle Technology Handbook (Elsevier, Amsterdam) 2007.

[11] Tartaj P, Morales MP, Gonzalez-Carreño V, Veintemillas-Verdaguer S, Serna CJ. Advances in magnetic nanoparticles for biotechnology applications. Journal of Magnetism and Magnetic Materials 2005; 290(1) 28-34.

[12] Beji Z., Ben Chaabane T., Smiri L.S., Ammar S., Fiévet F., Jouini N., and Grenèche J.M. Synthesis of nickel-zinc ferrite nanoparticles in polyol: morphological, structural and magnetic properties. physica status solidi (a) 2006; 203(3) 504-512.

[13] Tartaj P, Morales MP, Gonzalez-Carreño V, Veintemillas-Verdaguer S, Serna CJ. The preparation of magnetic nanoparticles for applications in biomedicine. Journal of Physics D: Applied Physics 2003; 36 R182.

[14] Dang F, Enomoto N, Hojo J, Enpuku K. A novel method to synthesize monodispersed magnetite nanoparticles. Chemical Letters 2008; 37(5) 530-531.

[15] Matsunaga T, Okamura Y, Tanaka T. Biotechnological application of nano-scale engineered bacterial magnetic particles. Journal of Materials Chemistry 2004; 14(14) 2099-2105.

[16] Guimaraes AP. Magnetism and magnetic resonance in solids. Wiley VCH (1998). (ISBN: 0471197742).

[17] Well JA, Bolton JR. Electron paramagnetic resonance: elementary theory and practical applications 2nd edition. John Wiley and Sons, 2007. (ISBN: 047175496X); Brustolon MR. Electron paramagnetic resonance: a practitioner toolkit, 1st edition. John Wiley and Sons (2009) (ISBN: 0470258829).

[18] Valenzuela R, Herbst F, Ammar S. Ferromagnetic resonance in Ni–Zn ferrite nanoparticles in different aggregation states. Journal of Magnetism and Magnetic Materials 2012; 324(21) 3398-3401.

[19] Guskos N, Zolnierkiewicz G ,Typek J, Guskos A, Czech Z. FMR study of γ-Fe2O3 agglomerated nanoparticles dispersed in glues. Reviews on Advanced Materials Science 2007;14 57-60.

[20] Thirupathi G, Singh R. Magnetic Properties of Zinc Ferrite Nanoparticles. Institute of Electrical and Electronics Engineers Transactions on Magnetics 2012; 48 3630-3633.

[21] De Biasi E, Lima E, Ramos C A, Butera A, Zysler R D. Effect of thermal fluctuations in FMR experiments in uniaxial magnetic nanoparticles: Blocked vs superparamagnetic regimes . Journal of Magnetism and Magnetic Materials 2013; 326(1) 138-146.

[22] Sobón M, Lipinski I E, Typek J, Guskos A. FMR Study of Carbon Coated Cobalt Nanoparticles Dispersed in a Paraffin Matrix. Solid State Phenomena 2007; 128 193-198.

[23] Shames A I, Rozenberg E, Sominski E, Gedanken A. Nanometer size effects on magnetic order in La12xCaxMnO3 (x = 0.5 and 0.6) manganites, probed by ferromagnetic resonance. Journal of Applied Physics 2012; 111 07D701-1-07D701-2.

[24] Owens F. Ferromagnetic resonance observation of a phase transition in magnetic field aligned Fe_2O_3 nanoparticles. Journal of Magnetism and Magnetic Materials 2009; 321(15) 2386-2391.

[25] Gazeau F, Bacri J C, Gendron F, Perzynski R, Raikher Yu L, Stepanov V I, Dubois E. Magnetic resonance of ferrite nanoparticles: Evidence of surface effects. Journal of Magnetism and Magnetic Materials 1998; 186(2) 175-187.

[26] Noginov M, Noginova N, Amponsah O, Bah R, Rakhimov R, Atsarkin V A. Magnetic resonance in iron oxide nanoparticles: Quantum features and effect of size. Journal of Magnetism and Magnetic Materials 2008; 320(18) 2228-2232.

[27] Gazeau F, Bacri J C, Gendron F, Perzynski R, Raikher Yu L, Stepanov V I, Dubois E. Magnetic resonance of nanoparticles in a ferrofluid: Evidence of thermofluctuational effects. Journal of Magnetism and Magnetic Materials 1999; 202(2-3) 535-546.

[28] Edelman I, Petrakovskaja E, Petrov D, Zharkov S, Khaibullin R, Nuzhdin V, Stepanov A. FMR and TEM studies of Co and Ni nanoparticles implanted in the SiO_2 matrix. Applied Magnetic Resonance 2011; 40 363-375.

[29] Martinez B, Obradors X, Balcells Ll, Rouanet A, Monty C. Low temperature surface spin-glass transition in gamma-Fe2O3 nanoparticles. Physical Review Letters 1998; 80 181-184.

[30] Winkler E, Zysler R D, Fiorani D. Surface and magnetic interaction effects in Mn3O4 nanoparticles. Physical Review B 2004; 70 174406-1-174406-5.

[31] Song H, Mulley S, Coussens N, Dhagat P, Jander V. Effect of packing fraction on ferromagnetic resonance in $NiFe_2O_4$ nanocomposites. Journal of Applied Physics 2012; 111 (07E348) 07E348_1 - 07E348_3.

[32] De Biasi R, Devezas T. Anisotropy field of small magnetic particles as measured by resonance. Journal of Applied Physics 1978; 49 2466-2470.

[33] Munir Z.A., Quach D.V. and Ohyanagi M. Electric current activation of sintering: a review of the pulsed electric current sintering process. Journal of the American Ceramic Society 2011; 94(1) 1-19.

[34] Anselmi-Tamburini U, Garay JE and Munir ZA. Fundamental investigation on the spark plasma sintering/synthesis process III. Current effect on reactivity. Materilas Science and Engineering A 2005; 407 24-30.

[35] Mizuguchi T, Guo S and Kagawa Y. Transmission electron microscopy characterization of spark plasma sintered ZrB2 ceramicc. Ceramics International 2010; 36(3) 943-946.

[36] Regaieg Y, Delaizir G, Herbst F, Sicard L, Monnier J, Montero D, Villeroy B, Ammar-Merah S, Cheikhrouhou A, Godart C, Koubaa M. Rapid solid state synthesis by spark plasma sintering and magnetic properties of $LaMnO_3$ perovskite manganite. Materials Letters 2012; 80(1) 195-198.

[37] Valenzuela R, Ammar S, Nowak S, and Vázquez G. Low field microwave absorption in nanostructured ferrite ceramics consolidated by spark plasma sintering. Journal of Superconductivity and Novel Magnetism 2012; 25(7) 2389-2393.

[38] Gaudisson T, Acevedo U, Nowak S, Yaacoub N, Greneche JM, Ammar S, Valenzuela R. Combining soft chemistry and Spark Plasma Sintering to produce highly dense and finely grained soft ferrimagnetic $Y_3Fe_5O_{12}$ (YIG) ceramics. (to be published).

[39] Nakamura T, Okano Y, Tabuchi M, Takeuchi T. Synthesis of hexagonal ferrite via spark plasma sintering technique. Journal of the Japan Society of Powder and Powder Metallurgy 2001; 48(2) 166-169.

[40] Valenzuela R, Beji Z, Herbst F, and Ammar S. Ferromagnetic resonance behavior of spark plasma sintered Ni-Zn ferrite nanoparticles produced by a chemical route. Journal of Applied Physics 2011; 109(*) 07A329-1-07A329-3.

[41] Sukhov A, Usadel KD, and Nowak U. Ferromagnetic resonance in an ensemble of nanoparticles with randomly distributed anisotropy axes. Journal of Magnetism and Magnetic Materials 2008; 320(1) 31-33.

[42] Ammar S, Jouini N, Fièvet F, Beji Z, Smiri L, Moliné P, Danot M, Grenèche JM. Magnetic properties of zin-ferrite nanoparticles synthesized by hydrolysis in a polyol medium. Journal of Physics: Condensed Matter 2006; 18(39), 9055-9069.

[43] Sui Y, Xu DP, Zheng FL and Su WH. Electrons spin resonance study of $NiFe_2O_4$ nanosolids compacted under high pressure. Journal of Applied Physics 1996; 80 719-723.

[44] A. Abragam and B. Bleaney, *Electron Paramagnetic Resonance of Transition Ions* (Clarendon Press, Oxford,1970).

[45] C. P. Poole and H. A. Farach, *Relaxation in Magnetic Resonance* (Academic Press, London, 1971).

[46] Koksharov Yu. A, Pankratov D A., Gubin SP, Kosobudsky ID, Beltran M, Khodorkovsky Y and Tishin AM. Electron Paramagnetic Resonance of Ferrite Nanoparticles. Journal of Applied Physics 2001;89 2293-2298.

[47] Kliava J and Berger R. Size and Shape Distribution of Magnetic Nanoparticles in Disordered Systems: Computer Simulations of Superparamagnetic Resonance Spectra. Journal of Magnetism and Magnetic Materials 1999; 205 328-342.

[48] Valenzuela R, Alvarez G, Montiel H, Gutiérrez MP, Mata-Zamora ME, Barrón F., Sanchez AY, Betancourt I, Zamorano R. Characterization of magnetic materials by low-field microwave absorption techniques. Journal of Magnetism and Magnetic Materials 2008; 320(14) 1961-1965.

[49] Montiel H, Alvarez G, Gutiérrez MP, Zamorano R, and Valenzuela R. The effect of metal-to-glass ratio on the low field microwave absorption at 9.4 GHz of glass coated CoFeBSi microwires. IEEE Transactions on Magnetics 2006; 42(10) 3380-3382.

[50] Montiel H., Alvarez G., Gutiérrez M.P., Zamorano R., and Valenzuela R. Microwave absorption in Ni-Zn ferrites through the Curie transition. Journal of Alloys and Compounds 2004; 369(1) 141-143.

[51] Prinz G.A., Rado G.T. and Krebs J.J. Magnetic properties of single-crystal {110} iron films grown on GaAs by molecular beam epitaxy. Journal of Applied Physics 1982; 53 (3) 2087-2091.

[52] Gerhardter F, Li Yi, and Baberschke K. Temperature-dependent ferromagnetic-resonance study in ultrahigh vacuum: magnetic anisotropies of thin iron films. Physical Review B 1993; 47(17) 11204-11210.

[53] Valenzuela R. The temperature behavior of resonant and non-resonant microwave absorption in Ni-n ferrites. In *Electromagnetic Waves* / Book 1, InTech Open Access

Publisher, edited by Vitaliy Zhurbenko, pp. 387 - 402 (2011), ISBN: 978 – 953 – 307 – 304 - 0. Online June 24, 2011 at: http://www.intechopen.com/articles/show/title/the-temperature-behavior-of-resonant-and-non-resonant-microwave-absorption-in-ni-zn-ferrites.

[54] Alvarez G., Montiel H., Barron J.F., Gutiérrez M.P., Zamorano R. Yafet-Kittel-type magnetic ordering in $Ni_{0.35}Zn_{0.65}Fe_2O_4$ ferrite detected by magnetosensitive microwave absorption measurements. Journal of Magnetism and Magnetic Materials 2009; 322(3) 348-352.

[55] Montiel H, Alvarez G, Betancourt I, Zamorano R. and Valenzuela R. Correlation between low-field microwave absorption and magnetoimpedance in Co-based amorphous ribbons. Applied Physics Letters 2005 ; 86(7) 072503-1-072503-3.

[56] Barandiarán M., García-Arribas, A., and de Cos, D. Transition from quasistatic to ferromagnetic resonance regime in giant magnetoimpedance. Journal of Applied Physics 2006; 99 103904-1-103904-4.

[57] Knobel M, Kraus L, and Vázquez M. Magnetoimpedance. Handbook of Magnetic Materials, edited by K.H.J. Buschow, Elsevier Amsterdam 2003; 15 497-563.

[58] Valenzuela R., Ammar S., Herbst F., Ortega-Zempoalteca R. Low field microwave absorption in Ni-Zn ferrite nanoparticles in different aggregation states. Nanoscience and Nanotechnology Letters 2011; 3(4) 598-602.

[59] Valenzuela R., Montiel H., Alvarez G., and Zamorano R. Low-field non-resonant microwave absorption in glass-coated Co-rich microwires. Physica Status Solidi A 2009; 4, 652-655.

[60] Valenzuela R. (Unpublished results)

[61] Broese van Groenou A., Schulkes J.A., and Annis D.A. Magnetic anisotropy in some nickel zinc ferrites. Journal of Applied Physics 1967; 38(3), 1133 (1967).

[62] Yafet Y. and Kittel, C. Antiferromagnetic arrangements in ferrites. Physical Review 1952; 87(2) 290-294.

[63] Alvarez G., Montiel H., Barrón J.F., Gutiérrez M.P. Zamorano R. Yafet-Kittel-type magnetic ordering on NiZnFe2O4 ferrite detected by magnetosensitive microwave absorption measurements. Journal of Magnetism and Magnetic Materials 2010; 322(3) 348-352.

[64] Alvarez G., Font R., Portelles J., Zamorano R., and Valenzuela R. Microwave power absorption as a function of temperature and magnetic field in the ferroelectromagnet $Pb(Fe1/2Nb)O_3$. Journal of the Physics and Chemistry of Solids 2007; 68(7) 1436-1442.